Journal Pre-proof

Adsorption of chrysene in aqueous solution onto MIL-88(Fe) and NH_2-MIL-88(Fe) metal-organic frameworks: kinetics, isotherms, thermodynamics and docking simulation studies

Zakariyya Uba Zango, Noor Hana Hanif Abu Bakar, Nonni Soraya Sambudi, Khairulazhar Jumbri, Nor Ain Fathiha Abdullah, Evizal Abdul Kadir, Bahruddin Saad

PII: S2213-3437(19)30667-0

DOI: https://doi.org/10.1016/j.jece.2019.103544

Reference: JECE 103544

To appear in: *Journal of Environmental Chemical Engineering*

Received Date: 18 September 2019

Revised Date: 11 November 2019

Accepted Date: 13 November 2019

Please cite this article as: Zango ZU, Abu Bakar NHH, Sambudi NS, Jumbri K, Abdullah NAF, Kadir EA, Saad B, Adsorption of chrysene in aqueous solution onto MIL-88(Fe) and NH_2-MIL-88(Fe) metal-organic frameworks: kinetics, isotherms, thermodynamics and docking simulation studies, *Journal of Environmental Chemical Engineering* (2019), doi: https://doi.org/10.1016/j.jece.2019.103544

Adsorption of chrysene in aqueous solution onto MIL-88(Fe) and NH_2-MIL-88(Fe) metal-organic frameworks: kinetics, isotherms, thermodynamics and docking simulation studies

Zakariyya Uba Zango[a], Noor Hana Hanif Abu Bakar[b], Nonni Soraya Sambudi[c], Khairulazhar Jumbri[a], Nor Ain Fathiha Abdullah[a], Evizal Abdul Kadir[d], Bahruddin Saad[a*]

[a]Fundamental and Applied Sciences Department, Universiti Teknologi PETRONAS, Seri Iskandar, Perak, Malaysia.

[b]School of Chemical Sciences, Universiti Sains Malaysia, Pulau Pinang, Malaysia.

[c]Chemical Engineering Department, Universiti Teknologi PETRONAS, Seri Iskandar, Perak, Malaysia.

[d]Faculty of Engineering, Universitas Islam Riau, Pekanbaru, Indonesia

[*]Corresponding author: bahruddin.saad@utp.edu.my

Highlights

- High porous and crystalline MIL-88(Fe) and NH_2-MIL-88(Fe) MOFs.
- Effective adsorption of Chrysene in aqueous solution onto the MOFs
- Shorter equilibration time of 25 minutes.
- Easy regeneration and re-usability of the MOFs for the chrysene adsorption.
- Molecular docking simulations for binding interactions between the MOFs with the CRY.

Abstract

MIL-88(Fe) and NH_2-MIL-88(Fe) metal-organic frameworks were synthesized using the microwave-assisted solvothermal method and were characterized using scanning electron microscopy (SEM), Brunauer Emmett Teller (BET), powdered X-ray diffraction (XRD) and Fourier transformed infrared (FTIR) spectroscopy. Relatively high surface areas with corresponding pore volumes of 1240 $m^2 g^{-1}$ and 0.7 $m^3 g^{-1}$, 941 $m^2 g^{-1}$ and 0.6 $m^3 g^{-1}$ were found for MIL-88(Fe) and NH_2-MIL-88(Fe), respectively. The MOFs were evaluated as adsorbent for the removal of chrysene (CRY) in water. Important parameters that affect the adsorption such as contact time, initial concentration of CRY, pH and temperature were systematically studied. Adsorption isotherms using Langmuir, Freundlich and Temkin models were investigated. Other details of the adsorption process were also studied using kinetics and thermodynamics approaches. Additionally, molecular docking was used to unravel the nature of the adsorption between the MOFs and CRY. The reusability of the adsorbents was evaluated using regeneration studies. In conclusion, these MOFs exhibit favorable characteristics to be used for the removal of CRY from water.

Keywords: Adsorption, Chrysene, Metal-Organic Frameworks, Removal, Regeneration

1.0 Introduction

Water contamination from pollutants resulting from natural and anthropogenic sources has been a topic of environmental concern for the last three decades. Organic pollutants resulting from industrial, mining and agricultural activities are often discharged into the water bodies and vast majority of them are highly toxic to humans, plants, and other living organisms [1,2].

Polycyclic aromatic hydrocarbons (PAHs) are among the toxic organic pollutants that are classified as endocrine disruptors. They comprise of two or more benzene ring molecules, forming highly stable structures [3,4]. Their wide occurrence in the environment are the consequences of human activities as a result of rapid industrialization, urbanization, and energy demand. They are generated through anthropogenic processes such as crude oil, exploration, incomplete combustion of petroleum and petrochemical products, coal, coke and carbon black production, wastewater discharge from petrochemical plants, leakage of engine oil, among others [5,6,7]. Chrysene (CRY, **Fig 1**) is a four-membered benzene ring PAH with a half-life of around 371-381 days [8]. It has been detected in various environmental samples in different parts of the world. Higher concentration of CRY (53,157 ± 20 mg kg^{-1}) was reportedly found in foam waste released from an aluminum industry [9]. The incidence of PAH in drinking water has raised much concern over decades due to its adverse health effects on living organisms. It binds with human DNA, resulting in carcinogenic and mutagenic reactions that are associated with severe health effects such as lung cancer, and reproductive defects [10,11,12].

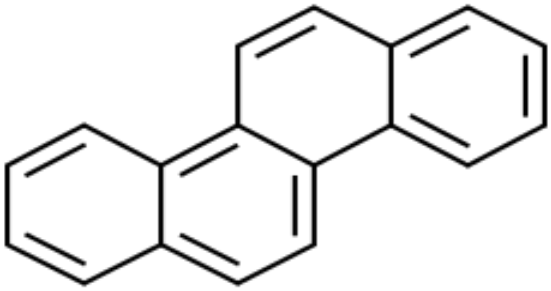

Fig 1. Chemical structure of chrysene

Wastewater remediation technologies over the last three decades have been dominated by coagulation, flocculation, and bioremediation [13,14]. However, incomplete removal, together with the formation of toxic secondary pollutants are often encountered [15]. Of the various technologies, adsorption has been identified as the best alternative practice [16,17]. Adsorbents materials such as biomass [19-22] activated carbons [23-25], polymers, biopolymers and molecularly imprinted polymer materials [26,21], graphene and graphene oxide [28-31], clay and modified clay minerals [32,33], carbon nanotubes [34-37], silica-based materials [38,39] have been extensively studied as possible replacement to the conventional adsorbents for wastewater remediations. The application of mussel inspired chemistry to modify the adsorbents to improve the adsorption capacity has also been proposed [40-42].

Metal-organic frameworks (MOFs) are ultra-high porous and high crystalline materials, consisted of inorganic and organic parts; with metal ions as the central atom and the organic moieties as the linkers. They formed frameworks of high tunability with sufficient number of pores

and cavities [43-45]. The diversity in the design of the frameworks and different synthesis routes, together with the chemical stability of the materials render them versatile for various applications [46,47]. MOFs containing iron as metal node (e.g., Fe-BTC, MIL-53(Fe), and MIL-68(Fe)) [48], offered remarkable high porosity, thermal and chemical stability, as well as moisture resistance. Thus, they could be employed as potential adsorbent materials for the removal of organic pollutants in wastewater.

In this work, we reported highly porous and stable Fe-based MOFs, i.e., MIL-88(Fe) and NH_2-MIL-88(Fe) as adsorbents for the removal of CRY in water. CRY was chosen as model analyte because of its adverse environmental impacts and toxicity to humans. Various factors affecting the adsorption; kinetics, isotherms, and thermodynamics of the process were evaluated. Possible reusability of the MOFs was also studied. Theoretical modeling of the interactions of the MOFs with the CRY was conducted using molecular docking tools.

2.0 Experimental Section

2.1 Chemicals and Materials

All chemicals used in this work were of analytical grade and were used as received. Iron (III) chloride, terephthalic acid, amino terephthalic acid and CRY were purchased from Sigma Aldrich (USA). Dimethylformamide (DMF), methanol, sodium hydroxide, and hydrochloric acid were supplied by Avantis Laboratory Malaysia.

2.2 Methodology

2.2.1 Synthesis of MIL-88(Fe) and NH_2-MIL-88(Fe)

The procedure for the synthesis of MIL-88(Fe) as described by Xu., et al., 2016 [49] was used in this work with minor modifications. It involved dissolving $FeCl_3 \cdot 6H_2O$ (0.8109 g, 3 mmol) and terephthalic acid (0.49839 g, 3 mmol) in 50 mL of DMF with vigorous stirring and sonication for 15 minutes and 10 minutes respectively. The solution was capped in a vial and placed in a microwave oven (140 watts) at 150℃ for 15 min. Cooling at room temperature resulted in the formation of brownish particles which were isolated by centrifugation at 4000 rpm for 10 minutes. The product formed was then washed with ethanol and deionized water to remove the organic solvents. Finally, it was dried at vacuum overnight at 70 °C.

Similar method was used in the synthesis of NH_2-MIL-88(Fe), by substituting the organic linker to amino terephthalic acid.

2.2.2. Characterizations

The synthesized MOFs were characterized using Fourier transformed infrared (FTIR) (Perkin Elmer FTIR spectrometer) for functional groups, scanning electron microscopy (SEM) for morphology and surface elemental determination (ZEISS, Ultra 55). N_2 adsorption-desorption (Micromeritics ASAP 2020) was used for BET surface area and pore volumes, powdered X-ray diffraction (XRD) (Bruker D8 Advance X-ray diffractometer) for crystallinity determination and thermogravimetry (Shimadzu TGA-50 Analyzer) for thermal stabilities.

2.3 Removal Experiment

2.3.1 Preparation of CRY solutions

Stock solution of CRY (20 mg L^{-1}) was prepared in acetone by dissolving 2 mg in 100 mL volumetric flask. It was kept in the refrigerator at 0 °C before use. Working solutions were prepared daily by diluting the required amount of the stock solution**.**

2.3.2 Batch adsorption study

Batch removal experiment was conducted by using 30 mL of CRY solution (4 mg L^{-1}) in a conical flask. The synthesized MOF (5 mg) was added to the solution and agitated at 200 rpm in an incubator shaker (Incubator ES 20/60, bioSan) at room temperature (25 °C). About 2 mL aliquot of the sample solution was collected at 5 minutes interval, filtered using nylon syringe membrane (0.4 μm) and the absorbance read at 374 nm with UV-visible spectrophotometer (GENESYS 30). Triplicate results were taken, and the average value was calculated.

The percentage removal (%R), quantity adsorbed at certain time interval (q_t), and quantity at equilibrium (q_e) were determined as follows:

$$\%R = \frac{C_0 - C_e}{C_0} \times 100 \quad (1)$$

$$q_t = \frac{(C_0 - C_t)V}{w} \quad (2)$$

$$q_e = \frac{(C_0 - C_e)V}{w} \quad (3)$$

where C_0, C_t, and C_e are the initial, time and equilibrium concentrations (mg L^{-1}), w is the adsorbent weight (g), and V is the volume of CRY used (L).

Different initial concentrations of CRY (1-5 mg L^{-1}) were studied. The amount of the adsorbents used were 5 mg and all other conditions were maintained. Similarly, the effect of the

pH of the solution (2-12) was investigated. CRY (4 mg L^{-1}) and MOF (5 mg) were used. The effect of temperature (25-45 °C) was studied under the same conditions to batch adsorption studies.

Regeneration of the adsorbents and their reusability were also studied. The adsorbents were regenerated after used by decanting the filtrate and washing the residual particles with absolute ethanol (100 mL) and distilled water, followed by vacuum drying for 3 hours at 100 ^{0}C.

2.4 Adsorption Isotherms

Isotherms according to the Langmuir, Freundlich and Temkin models were used to elucidate the interaction between the MOFs with CRY.

2.4.1. Langmuir isotherm

This model accounts for the effect of monolayer adsorption onto the adsorbent surface of a finite number of identical sites. It assumed that: (i) there is negligible force of interactions between the adsorbate molecules with the adsorbent, (ii) Occupation of adsorption sites leads to no further adsorptions, (iii) only specific homogenous adsorption sites of the adsorbent interacts with the adsorbent molecules, and (iv) adsorption became less efficient when the distance between the adsorbent and the adsorbate molecules became wider. It is mathematically expressed as [50]:

$$\frac{C_e}{q_e} = \frac{1}{K_L q_m} + \frac{1}{q_m} C_e \quad (4)$$

$$R_L = \frac{1}{1+C_o K_L} \quad (5)$$

where C_e is the concentration at equilibrium (mg g^{-1}), q_e is the quantity of CRY adsorbed at equilibrium (mg g^{-1}), q_m and K_L are constants representing the adsorption capacity and adsorption energy respectively. R_L (dimensionless) parameter explains the favorability of the adsorption process (R_L >1, unfavorable; 0 < R_L < 1, favorable; R_L = 1, linear).

2.4.2. Freundlich isotherm

This model explains non-identical adsorbent with heterogeneous surfaces. It gives a satisfactory description of the adsorption system with heterogenous surface energy. The model is expressed as:

$$\log(q_e) = \log K_F + \frac{1}{n_F}\log C_e \quad (6)$$

K_F is the Freundlich isotherm constant which represents the adsorption capacity. The value $1/n_F$, represents the adsorption intensity.

2.4.3. Temkin isotherm

This model considers indirect interaction between adsorbate molecules and the adsorbent and explains how the heat of adsorption decreases with coverage.

Mathematically it is given as:

$$q_e = \frac{RT}{b_T} \ln A_T C_e \quad (7)$$

b_T represents the Temkin heat of adsorption, (kJ mol^{-1}). A is the binding constant at equilibrium corresponding to the maximum binding energy (L g^{-1}). T is the absolute temperature (K), while R is the Universal gas constant (8.314 J mol^{-1} K^{-1}).

These models were further fitted using statistical regression analysis to determine the coefficient of determination (R^2), adjusted coefficient of determination (R^2 adj), root means square error (RMSE) and Akaike information criterion (AIC) [51]:

$$R^2 = \left(\frac{\sum_h^i (q_{i\,exp} - \overline{q}_{i\,exp})^2 - \sum_h^i (q_{i\,exp} - \overline{q}_{i\,exp})^2}{\sum_n^i (q_{i\,exp} - \overline{q}_{i\,exp})^2}\right) \quad (8)$$

$$R^2adj = 1 - (1 - R^2)(\frac{n-1}{n-p}). \quad (9)$$

$$RMSE = \sqrt{\sum_{n=1}^{i}(q_{i\,exp} - q_{i\,model})^2} \quad (10)$$

$$AIC = nln\left(\frac{SSE}{n}\right) + 2n_p + \frac{2n_p(n_p+1)}{n(n_p+1)} \quad (11)$$

The q_e exp is the adsorption capacity that is determined experimentally, while the $\overline{q}e$ exp is the average experimental q_e. The q_e model is the calculated adsorption capacity generated from the model, n represents the number of experimental points, and p is the number of parameters of the fitted model.

2.5 Kinetics Study

Kinetics study is employed to explain the mechanism as well as the rate-controlling step which determine the efficiency of the adsorption [52]. In this study, the three most important kinetic models; i.e., pseudo-first-order, pseudo-second-order, and intra-particle diffusion were considered. The equations to represent the models are expressed by as follows [53,54]:

2.5.1 The pseudo-first-order kinetic model

$$q_t = q_e(1 - \exp(k_1 t)) \quad (12)$$

The q_e and q_t (mg g^{-1}) in the equation represent the amount of the CRY adsorbed at equilibrium and certain time (minutes), respectively. The k_1 (min^{-1}) is the pseudo-first-order rate constant.

2.5.2 The pseudo-second-order kinetic model

$$q_t = \frac{t}{(1/k_2 q_2)^2 + \left(\frac{t}{q_2}\right)} \quad (13)$$

Where k_2 (g $mg^{-1}min^{-1}$) is the pseudo-second-order rate constant.

2.5.3 Intra-particle diffusion model

$$q_t = K_P t^{\frac{1}{2}} + C \quad (14)$$

Where K_P ($mgg^{-1}min^{-1}$) is the intra-particle diffusion rate constant [55].

2.6 Thermodynamics study

The thermodynamics study provides information about the nature of the adsorption process with temperature changes. The parameters involved includes; Gibbs free energy change (ΔG°), enthalpy change (ΔH°) and entropy change (ΔS°) of the adsorption process. They were calculated from the equations [56]:

$$\Delta G° = -RTInK_C \quad (15)$$

$$\Delta G° = \Delta H° - T\Delta S° \quad (16)$$

where K_c is the distribution coefficient which represents the ratio of the quantity of CRY at the surface of the MOFs materials (Cads) to equilibrium concentration (C_e) of the CRY.

2.7 Molecular Docking simulation

Molecular docking is a simulation tool to measure the interaction between molecules that formed complexes. In this study, the interactions of the MOFs as the primary molecules with the CRY as the guest molecule is modeled. The crystal structure of MIL-88(Fe) and NH_2-MIL-88(Fe)

were obtained from Cambridge Crystallographic Data Centre (CCDC) and the CRY was retrieved from Automated Topology Builder (ATB) server [57]. The MIL-88(Fe) and NH_2-MIL-88(Fe) were modeled as a single unit cell and the CRY molecule was optimized by DFT method at B3LYP/6-31G* level of theory. All the molecules were prepared and saved as PDBQT file format to be further used for docking calculation.

The docking simulation was performed using AutoDock 4.2 software by running the Autogrid and AutoDock calculation. In Autogrid, CRY molecule was introduced into MIL-88(Fe) and NH_2-MIL-88(Fe) cavity. A grid box of 90 x 90 x 90 Å and 80 x 80 x 80 Å with a grid spacing of 0.425 Å were generated for MIL-88(Fe) and NH_2-MIL-88(Fe) respectively, to cover the entire surface of MOFs. To identify the appropriate binding modes and conformation for CRY molecule, the Lamarckian Genetic Algorithm (LGA) [58] from MGLTools was employed. Both MOFs were kept as a rigid framework and CRY was set as flexible around the surface of the MOFs during the conformational search. The binding energies between MIL-88(Fe) and NH_2-MIL-88(Fe) with CRY were calculated in AutoDock. The lowest energy conformer was selected.

$$\Delta G_{bind} = \Delta G_{VDW} + \Delta G_{electrostatic} + \Delta G_{HBond} + \Delta G_{desolv} + \Delta G_{tor} \quad (17)$$

where ΔG_{VDW} refers to van der Waal energy, $\Delta G_{electrostatic}$ refers to electrostatic energy, ΔG_{HBond} represent hydrogen bonding energy, ΔG_{desolv} represents desolvation energy and ΔG_{tor} is torsional free energy.

The inhibition constants (K_i) were calculated by the following equation:

$$K_i = e^{\left(\frac{\Delta G_{bind}}{RT}\right)} \quad (18)$$

3.0 Results and Discussions

3.1 Characterizations of MIL-88(Fe) and NH_2-MIL-88(Fe)

The FTIR spectra of the two MOFs were similar, except for the presence of peaks at 3500 cm^{-1} and 3200 cm^{-1} for MIL-88(Fe) which was attributed to the N-H stretching of the amino group in amino terephthalic acid **(Fig 2)**. The sharp peak at 1656 cm^{-1} is due to the C=O bond in the linkers of the MOFs. The peaks at 1396 cm^{-1} is assigned to symmetric vibrations of C-O of the carboxyl group in both MIL-88(Fe) and NH_2-MIL-88(Fe) [59][59][59]. Peaks at 683 cm^{-1} are assigned to the in-plane and out plane bending of -COO groups in the organic linkers of the MOFs. Bending vibrations due to O-Fe-O in the MOFs were observed at 516 cm^{-1} [60].

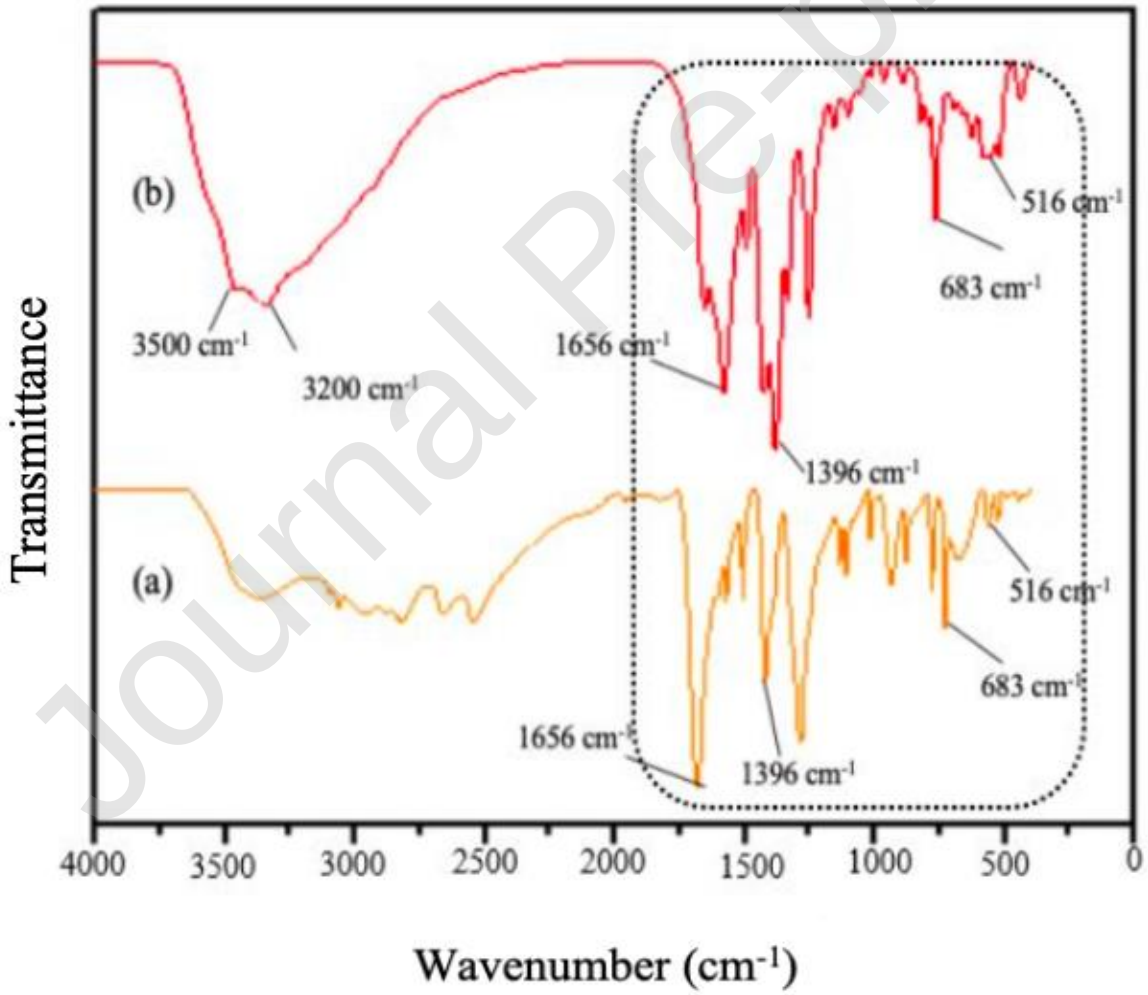

Fig 2. FTIR spectrum of (a) MIL-88(Fe) and (b) NH_2-MIL-88(Fe) MOFs

The SEM images of the MOFs are shown in **Fig 3(a-b)**. Spindle-like particles can be seen on the surfaces of the MOFs. No changes in the structural morphology of both MOFs was found even when exposed for 2 days under strong acidic condition (pH 1) as shown in **Fig 3(c-d)**. The spindle like-shape is typical of highly crystalline Fe-based MOFs such as MIL-53(Fe) [61] and MIL-101(Fe) [62]. The surface elemental compositions depicted by EDX results **is shown in Fig 4**. Both contained C, O, and Fe. However, the N peak of the amine functional group in NH_2-MIL-88(Fe) was not observed. It could have been shielded by C atoms in the organic linker. Trace amount of Cl observed at the surface of the MOFs could be due to the metal-salt that does not precipitate out during synthesis.

XPS results revealed that the surface of the MOFs contains iron (Fe2p), carbon (C1s) and oxygen (O1s). Additionally, nitrogen (N1s) peak was observed at the surface of NH_2-MIL-88(Fe) due to its amine functional group. The two MOFs have similar XRD pattern (**fig S1**), showing their high crystallinity that are typical of the Fe-based MOFs as previously reported [63].

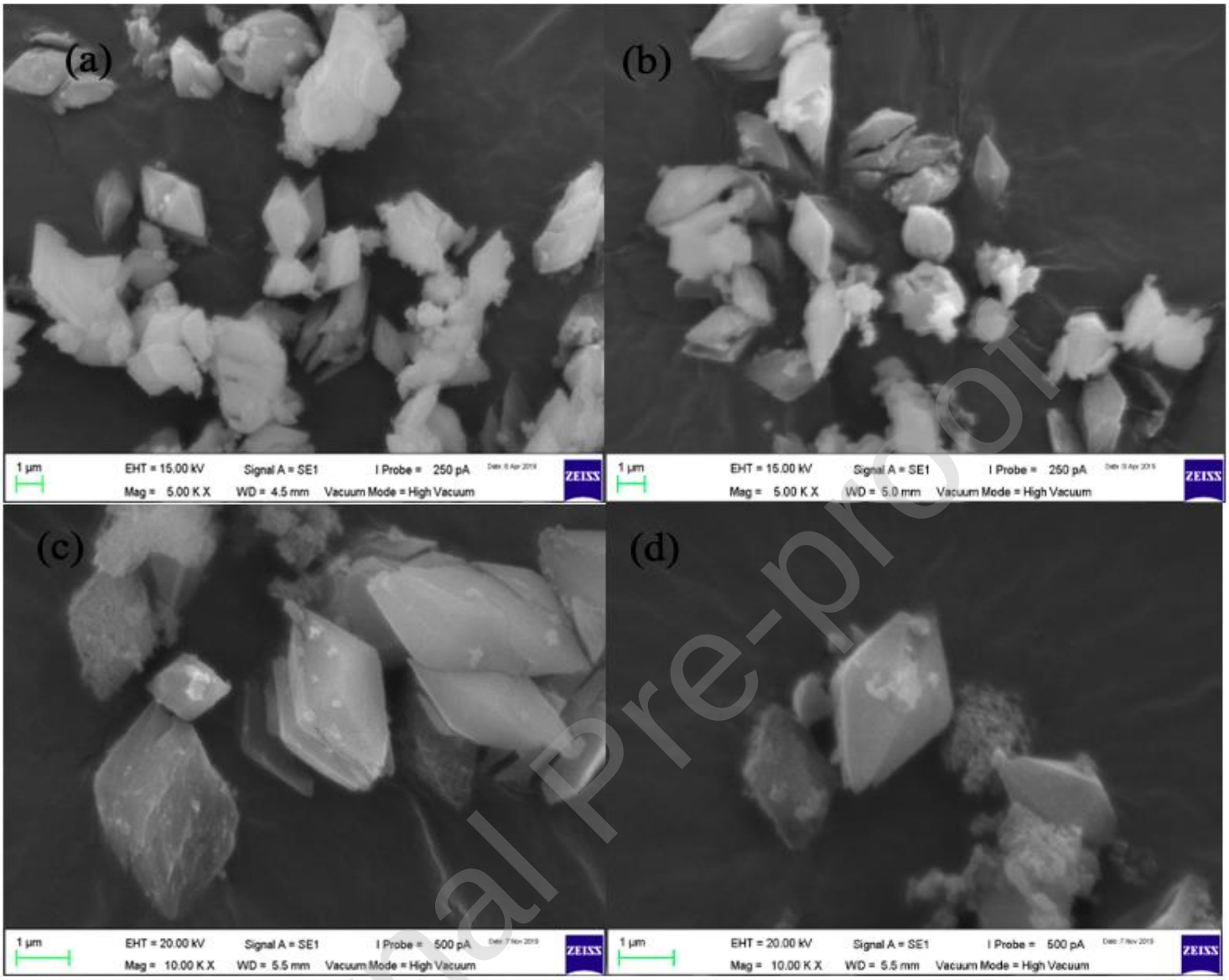

Fig 3. SEM images of as-synthesized MIL-88(Fe) and NH_2-MIL-88(Fe) (a and b) (5 KX), and (c-d) when exposed to pH 1 conditions for two days (10 KX)

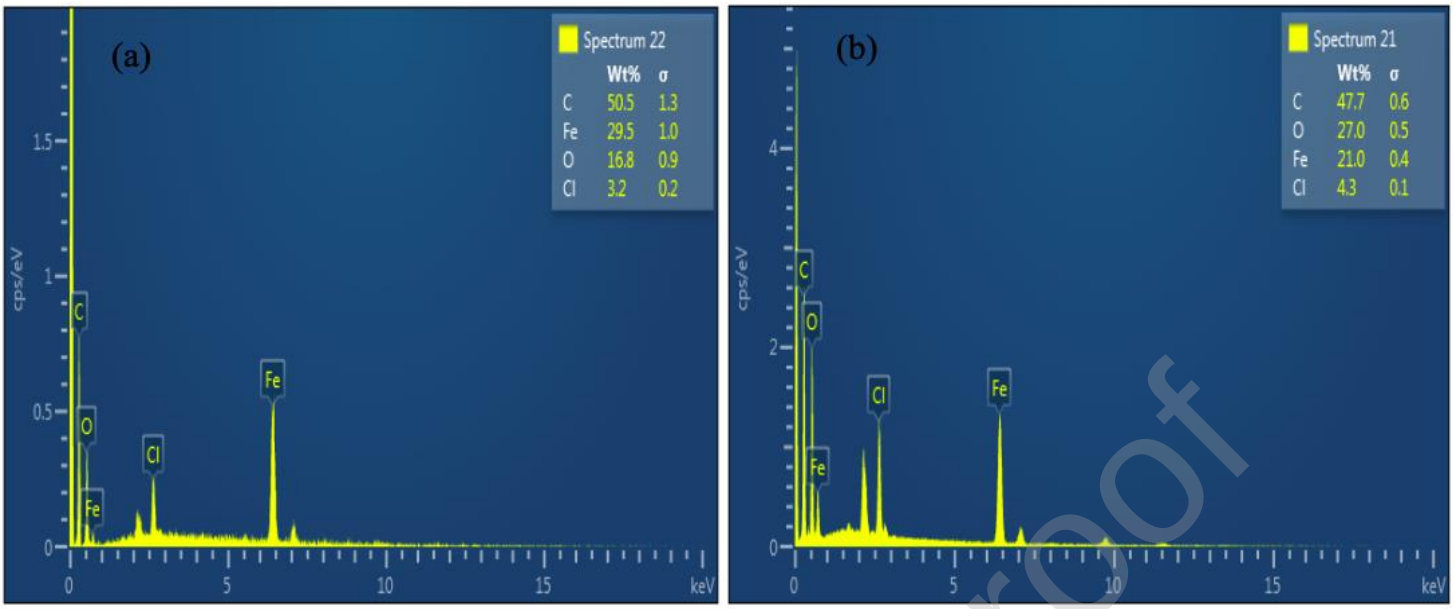

Fig 4. EDX spectrum of (a) MIL-88(Fe) and (b) NH_2-MIL-88(Fe)

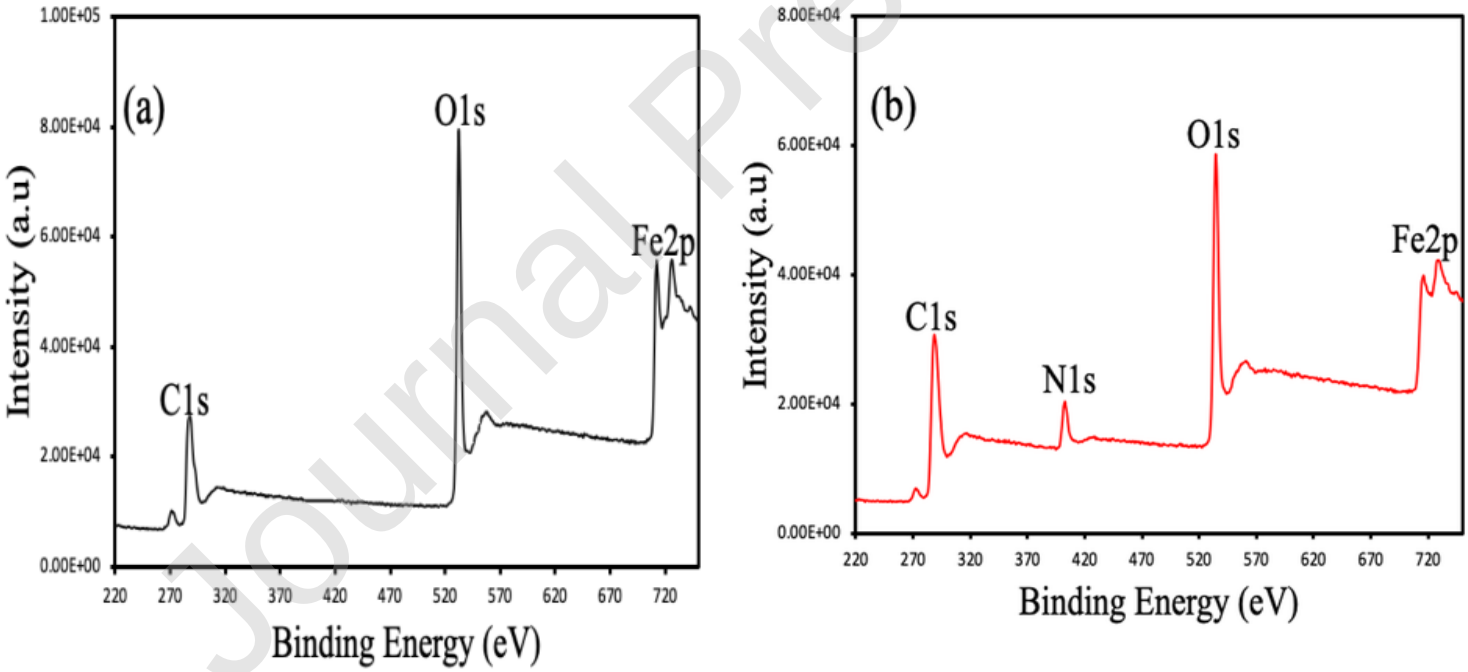

Fig 5. XPS spectrum of (a) MIL-88(Fe) and (b) NH_2-MIL-88(Fe)

Results for the surface areas, pore volumes, and pore sizes are shown in **table 1**, depicting the typical characteristics of porous materials. The higher BET surface area and pore volumes of MIL-88(Fe) compared to NH_2-MIL-88(Fe) is probably due to the amine group in NH_2-MIL-88(Fe) which occupies some of the empty spaces in the MOF.

3.2 Removal Studies

Good adsorbent materials are expected to achieve higher removal of the adsorbates even at lower dosage within the shortest possible time. As depicted by **fig 6,** rapid removal was achieved in 25 minutes with the MIL-88(Fe) and NH_2-MIL-88(Fe) MOFs (%R, 98.9±1.83 and 95.2±1.0% respectively). The adsorption capacities for MIL-88(Fe) and NH_2-MIL-88(Fe) were 23.6±0.001 and 22.2±0.001 mg g^{-1}, respectively. The higher adsorption capacity of MIL-88(Fe) MOF was probably due to its higher surface area as compared to the NH_2-MIL-88(Fe).

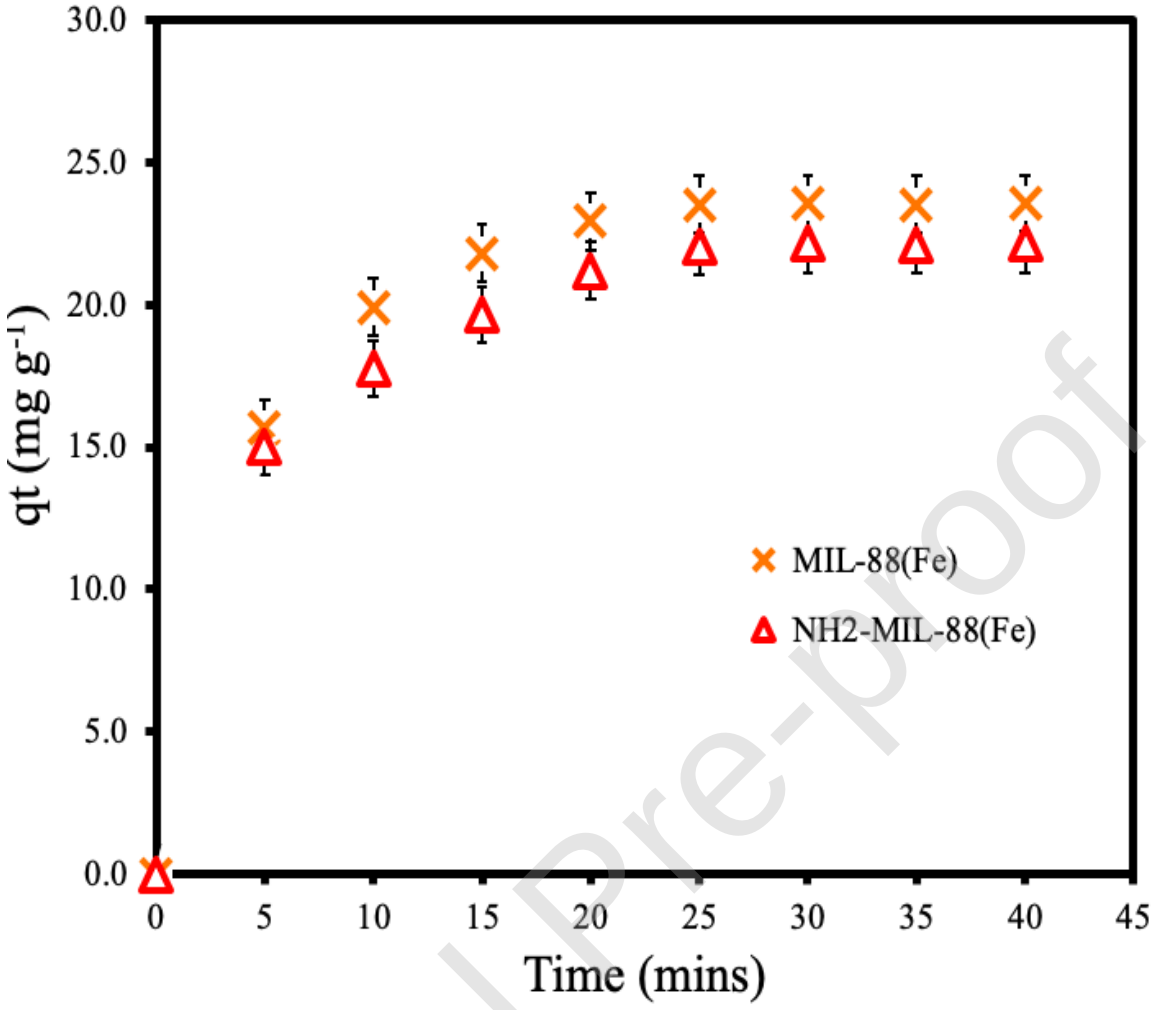

Fig 6. Effect of contact time for the adsorption of CRY onto the MIL-88(Fe) and NH_2-MIL-88(Fe) MOFs (4 mg L^{-1} CRY concentration, 5 mg of MOF, 25±0.1 °C and 200 rpm)

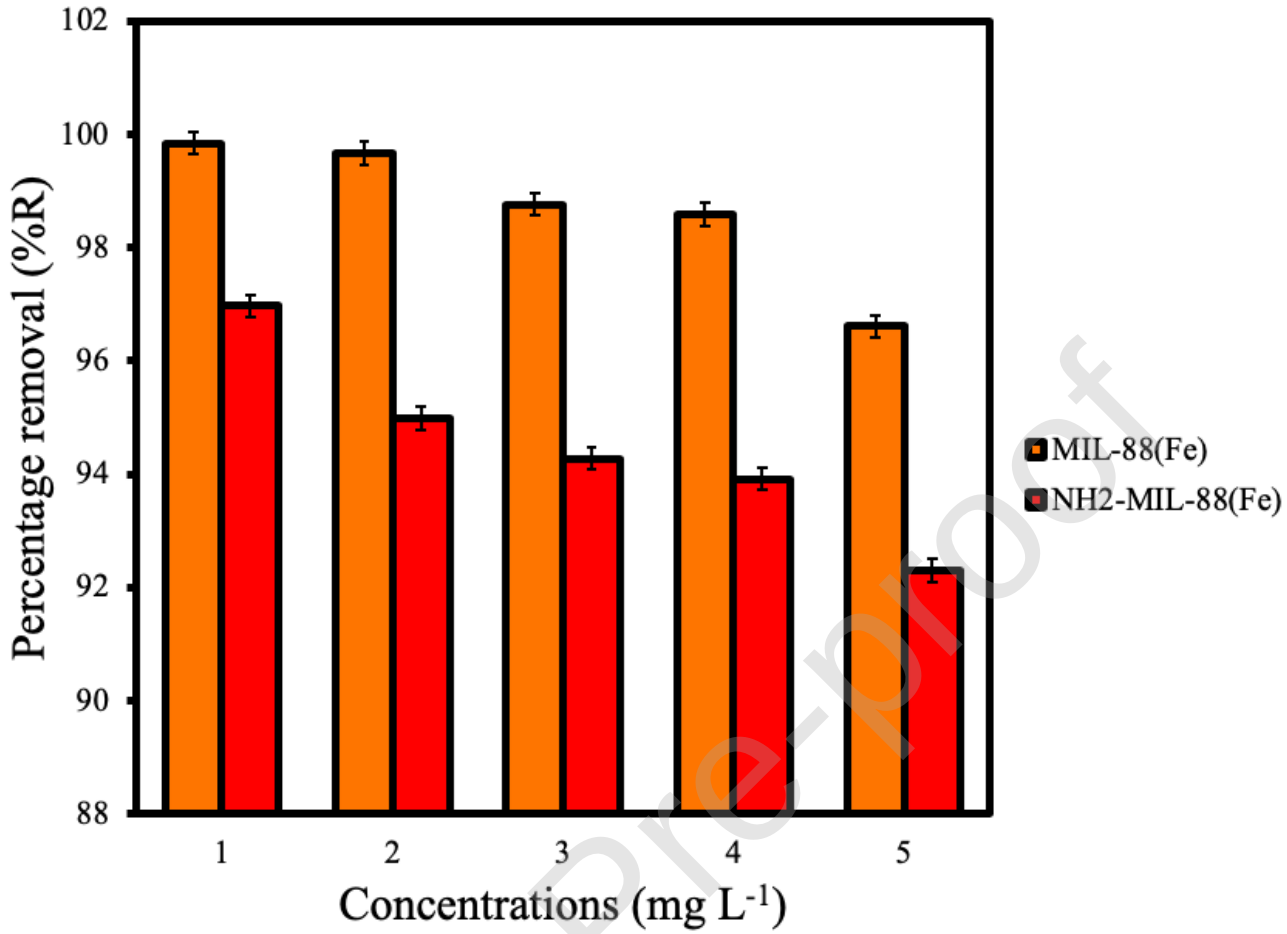

Fig 7. Adsorption of CRY at various concentrations onto the MIL-88(Fe) and NH_2-MIL-88(Fe) MOFs (1-5 mg L^{-1} of CRY, 5 mg of the MOF at 25±0.1 ˚C and 200 rpm)

The removal efficiency for different concentrations (1-5 mg L^{-1}) of CRY is shown in **Fig 7**. The %removal by MIL-88(Fe) was from 97.3±1.0 to 99.9±0.0% and for NH_2-MIL-88(Fe) was from 93.8±3.2 to 97.7±0.0% At 4 mg L^{-1}, the % removals were 98.9±1.8 and 95.2±1.0 % for MIL-88(Fe) and NH_2-MIL-88(Fe) respectively. Thus, for the rest of the study, 4 mg L^{-1} was arbitrarily chosen as the initial concentration of CRY.

The pH of the solution at which adsorption occurs plays an important role in the determination of adsorption efficiency. The pH influence on the adsorption study is illustrated in **Fig 8**. The removal efficiency was more favored by acidic pH for both MOFs. Previously, Sponza et al., (2011) and Abbasi et al., (2014) also reported higher removals of PAHs at acidic pH [38,39]. This was explained by the protonation of the PAHs molecules at acidic medium despite being neutral species.

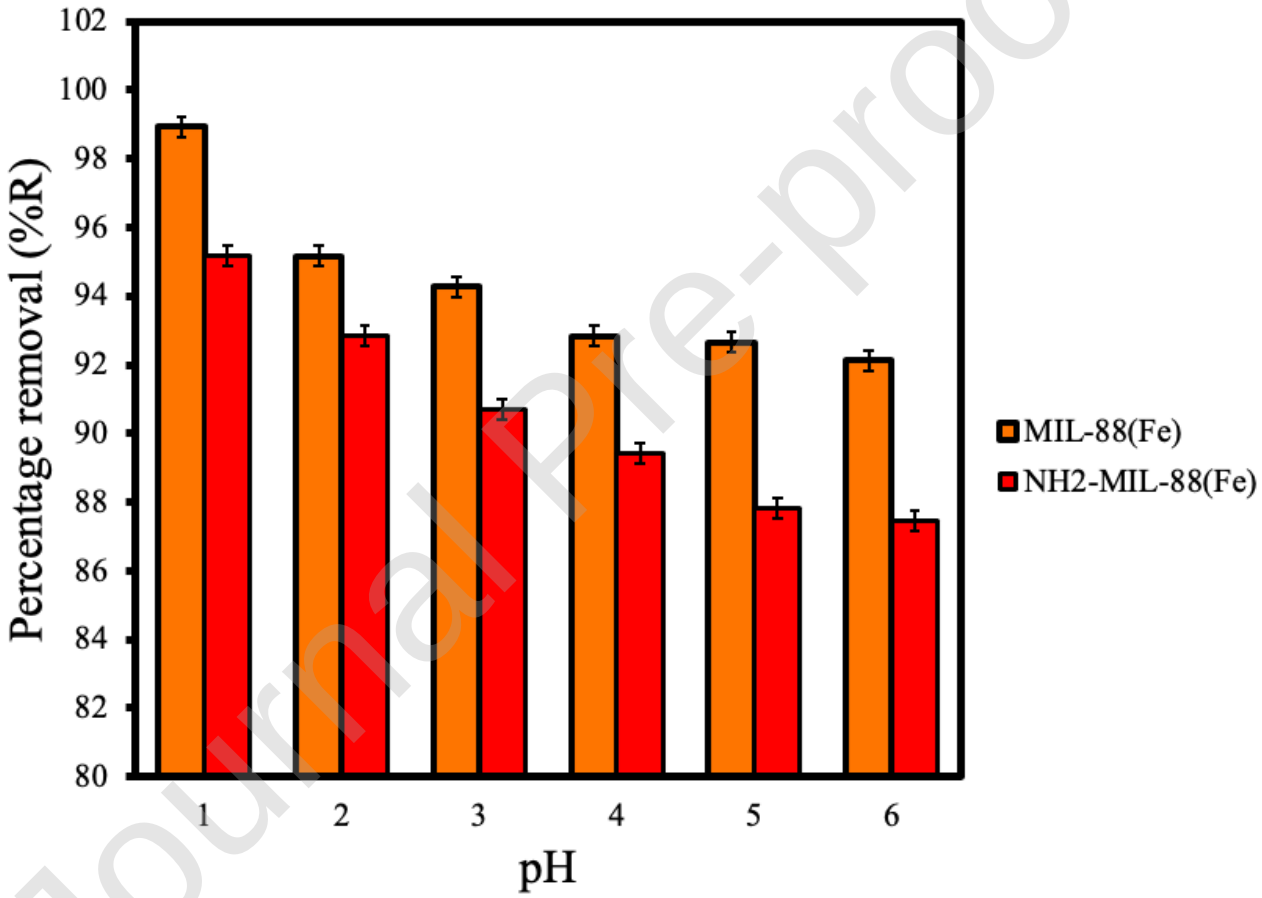

Fig 8. Effect of pH on the adsorption of CRY onto the MIL-88(Fe) and NH_2-MIL-88(Fe) MOFs (4 mg L^{-1} of CRY, 5 mg of the MOF at 25±0.1 $^{\circ}$C and 200 rpm)

From the plot of the q_e (mg g^{-1}) against T(K), the removal efficiency of CRY by both MOFs decreased at higher temperatures. This behavior is attributed to the decreased in surface coverage as the temperature is increased. Also, the lower adsorption capacity at higher temperature implies that the process is exothermic.

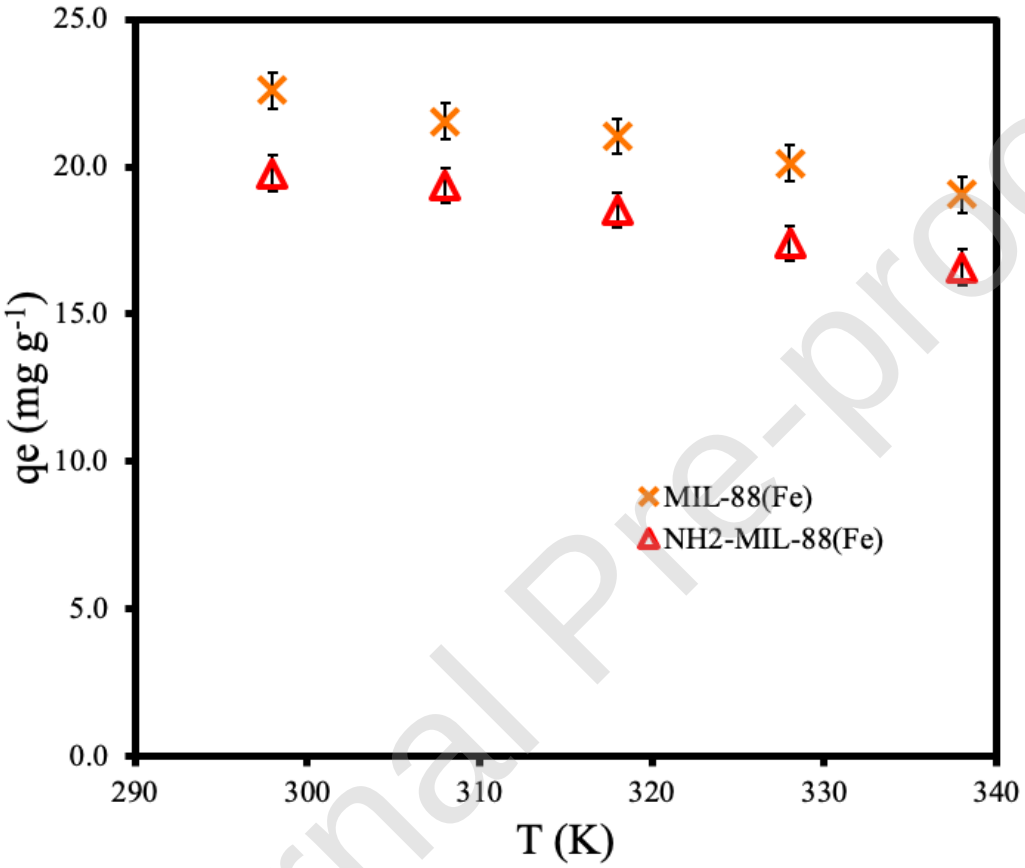

Fig 9. Effect of temperatures on the adsorption of CRY onto the MIL-88(Fe) and NH_2-MIL-88(Fe) MOFs (4 mg L^{-1} of CRY, 5 mg of the MOF at 25±0.1 °C and 200 rpm)

3.4 Isotherms studies

The adsorption isotherm models for the two MOFs are shown in **fig 10**. The values of the parameters are highlighted in table (S1). Langmuir model was the best to explain the good interactions of the adsorbate molecules with the MOFs based on the values obtained and the

regression analysis. The R_L values obtained were less than unity, (0.080 and 0.23) for MIL-88(Fe) and NH_2-MIL-88(Fe), respectively, which implies the favorable nature of the adsorption process. It was previously reported that π- π interactions and Van der Waals forces were the predominant driving force for the adsorption of aromatic compounds such as phenols and that both Langmuir and Freundlich were suitable to describe their isotherm behavior [66,67].

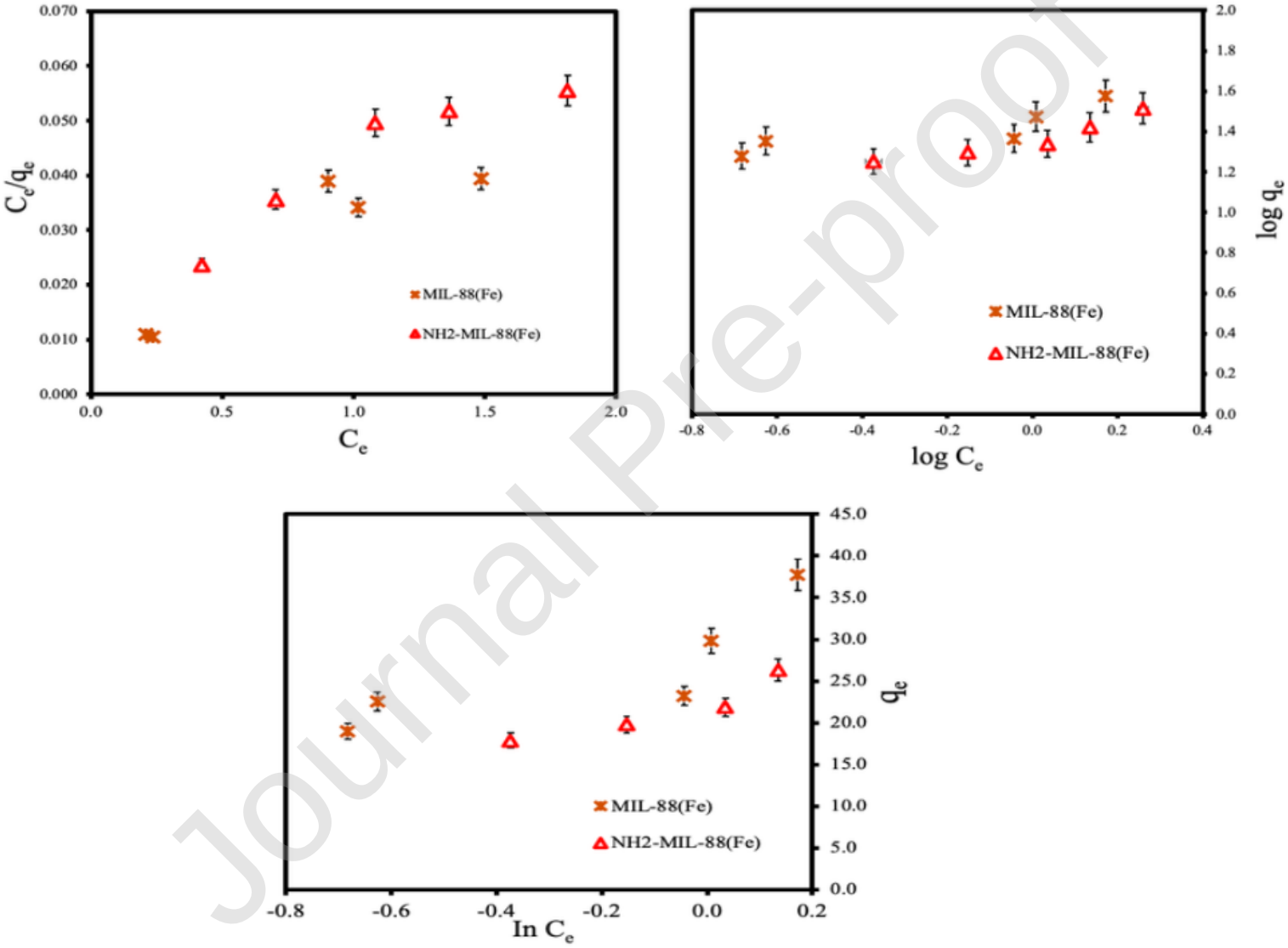

Fig 10. Isotherm plots for the removal of CRY by the MOFs, (a) Langmuir, (b) Freundlich and (c) Temkin.

3.5 Kinetic studies

Adsorption kinetic parameters using the various models are shown in Table 2. The pseudo-second-order model best supports the adsorption data with better coefficient of determinations (R^2), and root mean square errors (RMSE). Also, the calculated q_e (mg g^{-1}) values are closer to that of the experimental [68]. The intra-particle model explains the rate at which the adsorption takes place. In fig (S3), two basic steps could be seen. The first step is faster, depicting the external diffusion of the CRY molecules onto the surfaces of the MOFs. The second step is relatively slower, and it is attributed to the CRY adsorption onto the internal pores of the MOFs.

3.6 Thermodynamics studies

Thermodynamic parameters, namely Gibbs free energies (ΔG°), enthalpy changes (ΔH°) and entropy changes (ΔS°) explain the nature of the adsorption process. As highlighted in **table 3**, the ΔG° values obtained at various temperatures are negative and increased with temperatures. For MIL-88(Fe), the ΔH° and ΔS° values are -28.31 KJ mol^{-1} and -57.86 J mol^{-1} K^{-1}, respectively. Similarly, for the NH_2-MIL-88(Fe), the corresponding values for the ΔH° and ΔS° are 15.18 KJ mol^{-1} and -20.69 J mol^{-1} K^{-1}, respectively. The negative values for all the parameters confirmed the exothermic and favorable and spontaneous nature of the adsorption process at lower temperatures [69].

3.7 Adsorbent regeneration and reuse

The ease in recovery of the MOFs after the successful completion of the batch adsorption experiments demonstrates their potential as adsorbent for the removal of CRY. The % R achieved by MIL-88(Fe) at the 5th cycle was 84.9±3.77 % compared to 80.3±2.40% . for NH_2-MIL-88(Fe)

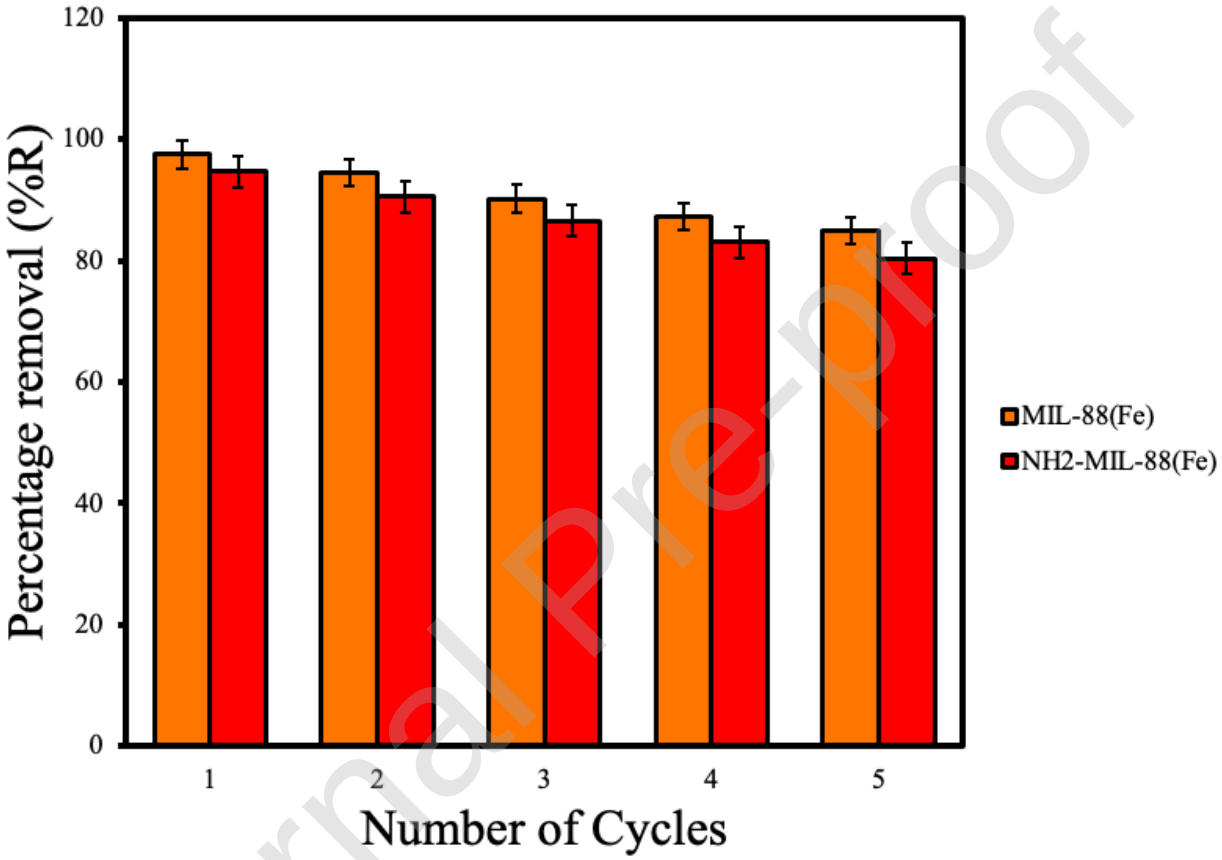

Fig 11. Regeneration studies for the adsorption of CRY by the MOFs

3.8 Comparison with other adsorbents

Table 4 compares the pertinent characteristics of adsorbents that had been reported for the removal of CRY from water. It is readily apparent from the table that the MOFs exhibit superior %R (95.2±1.00 and 98.9±1.83%), for MIL-88(Fe) and NH_2-MIL-88(Fe) respectively. The

equilibrium time was short (25 mins) and the adsorbents can be easily regenerated. It must be pointed out that regeneration studies were not discussed in most of the reported articles. Maximum adsorption capacities (Q_{max}) is also provided, although direct comparison is not possible due to the differences in experimental conditions that were used by the authors.

3.8 Molecular interactions

Molecular docking calculation was modeled to find the fundamental and theoretical interactions between the MIL-88(Fe) and NH_2-MIL-88(Fe) MOFs with the CRY molecule. The binding energy, intermolecular energy, and the inhibition constant are highlighted in Table S2. The binding energy represents the strength and stability of the inclusion complex formed between the CRY molecules with the MOFs. The higher negative value of binding energy implies the highest stability of the inclusion complex. The most stable structure was observed between MIL-88(Fe) and CRY with binding energy (ΔG_{bind}) of -3.82 Kcal mol^{-1} compared to -3.80 Kcal mol^{-1} for NH_2-MIL-88(Fe). Similarly, the inhibition constant obtained for MIL-88(Fe)(CRY) was slightly lower (1.58 mM) than that of NH_2-MIL-88(Fe)(CRY) (1.65 mM). This observation implies that MIL-88(Fe) has a slightly higher binding affinity towards CRY molecule. This was further supported by the higher BET surface area and pore size of MIL-88(Fe) as shown in **table 1**. The addition of an amine-functional group in NH_2-MIL-88(Fe) might occupy the available space inside the pristine MIL-88(Fe) adsorbent [73].

The corresponding lowest energy conformer of docking structures for MIL-88(Fe)(CRY) and NH_2-MIL-88(Fe)(CRY) were obtained and depicted in **Fig 12 and 13** respectively. Notably, the CRY molecule prefers to bind inside MIL-88(Fe) pore as the CRY molecule intrudes the pore conspicuously **(fig 12)**. On the contrary, in the case of NH_2-MIL-88(Fe), the CRY molecule

favorably binds along the outer space of the pores **(fig 13)**. This difference in preferable adsorption site occupied by CRY molecule might be due to the bigger pore size of MIL-88(Fe) (12.5 nm) than NH_2-MIL-88(Fe) (8.8 nm). There is no hydrogen bonding interaction observed between CRY molecule with both MIL-88(Fe) and NH_2-MIL-88(Fe) adsorbent respectively, due to the non-polar site of CRY molecule. It is noteworthy to point out that both MIL-88(Fe) and NH_2-MIL-88(Fe) adsorbents exhibit effective adsorption of CRY. All the docking simulation results are consistent with the experimental findings.

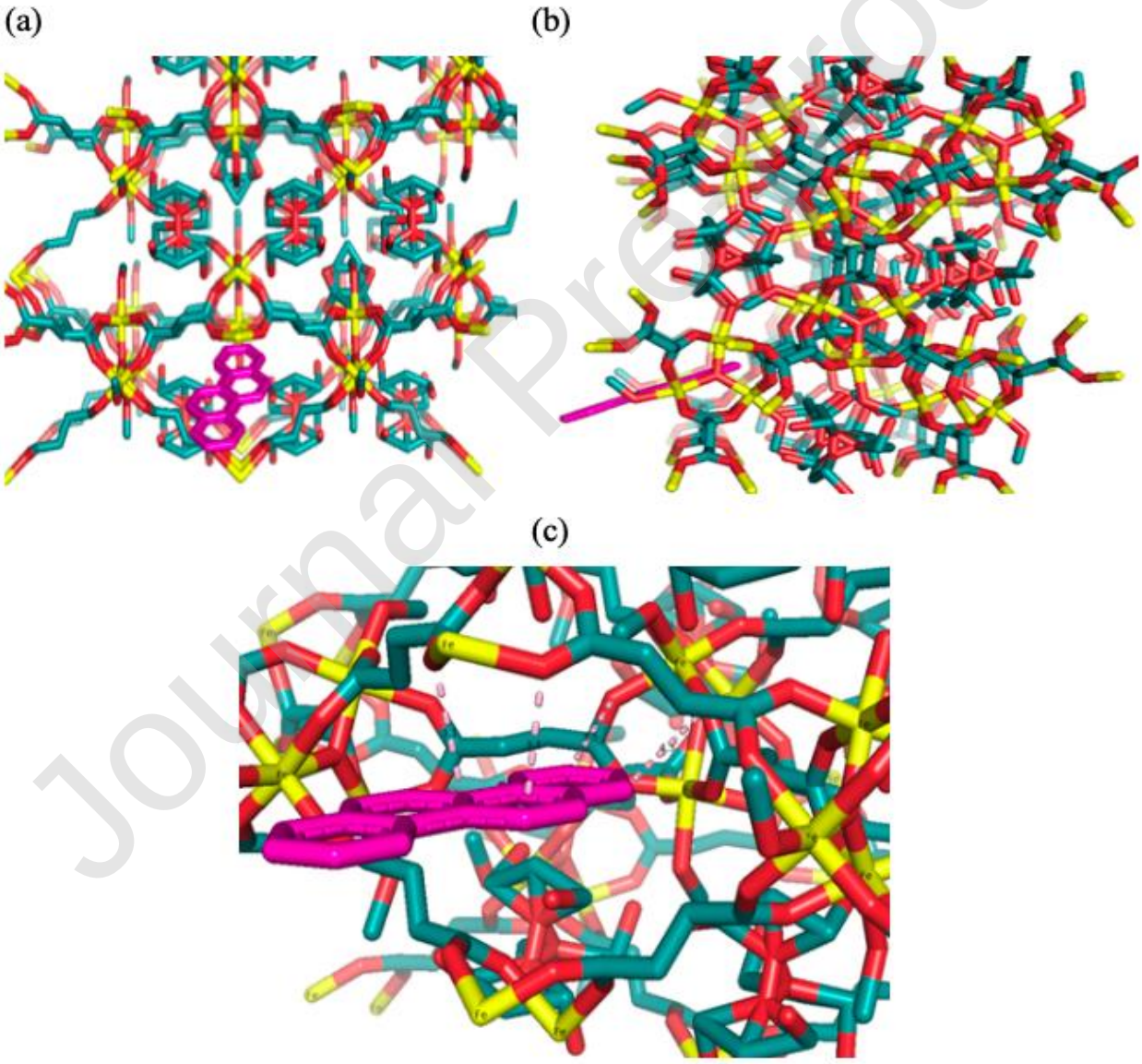

Fig12. The molecular docking structure of MIL-88(Fe)(CRY) complex at (a) Top view (b) Side view) (c) Zoom view. Metal (Fe), carbon (C), and oxygen (O) are colored as yellow, green, and red respectively.

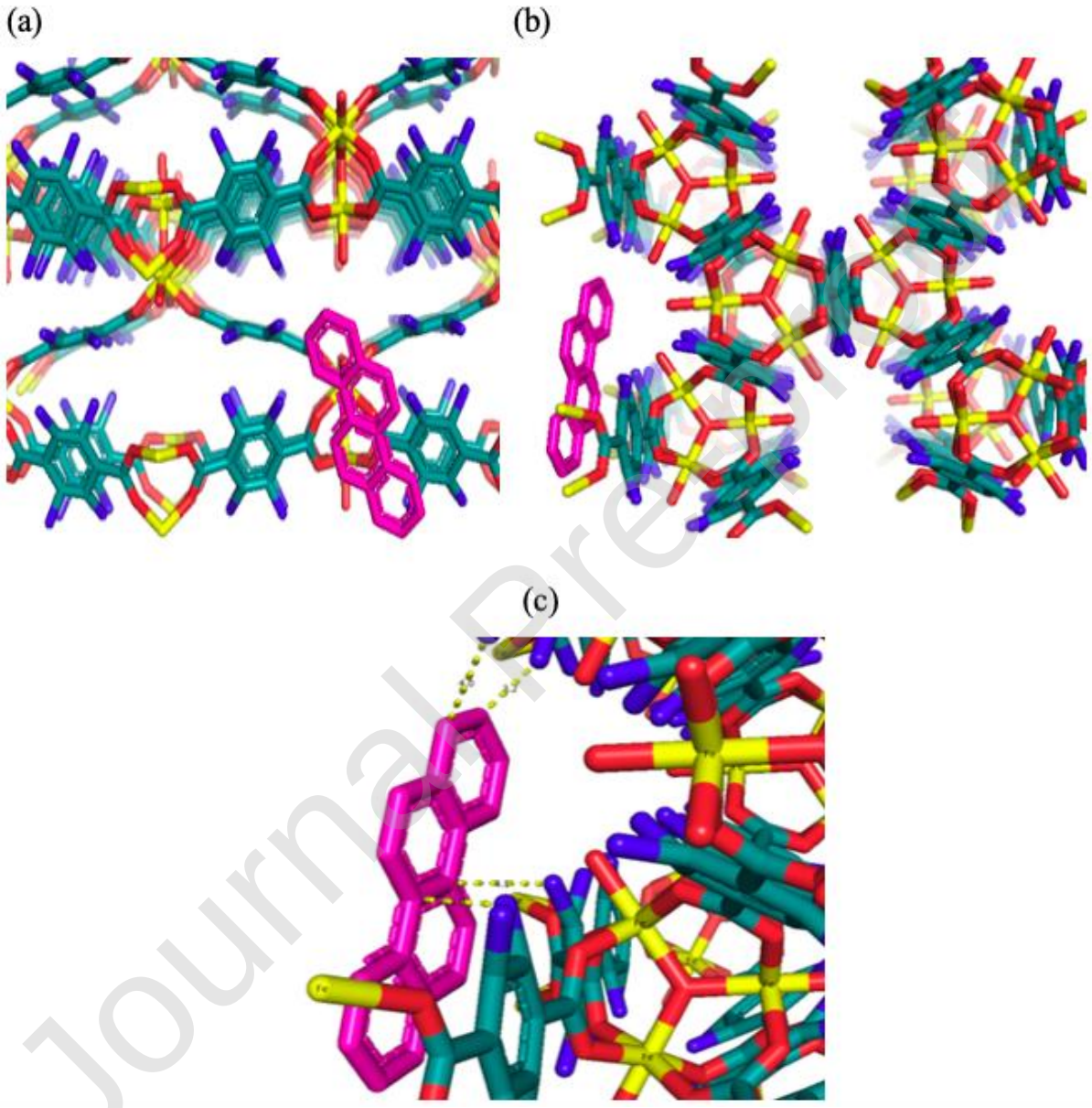

Fig 13. The molecular docking structure of NH_2-MIL-88(Fe)(CRY) complex at (a) Top view (b) Side view) (c) Zoom view. Metal (Fe), carbon (C), oxygen (O) and nitrogen (N) are colored as yellow, green, red and blue respectively.

4.0 Conclusions

Fe-based MOFs MIL-88(Fe) and NH_2-MIL-88(Fe) have been synthesized via microwave-assisted solvothermal method. Surface morphology shows the spindle-like particles at the surface of the MOFs. The BET surface area of MIL-88(Fe) and NH_2-MIL-88(Fe) were 1240 and 941 m^2 g^{-1}, while the corresponding pore volumes were 0.7 and 0.6 m^3 g^{-1} respectively. High crystallinity of the frameworks was demonstrated by the XRD patterns. Adsorption of CRY onto MIL-88(Fe) was found to be of 98.9±1.83, while that of NH_2-MIL-88(Fe) was found to be 95.2±1.00%. The regeneration and reusability of the MOFs onto CRY adsorption is reflected by the %R of 84.9±3.77 and 80.3±2.389% by the MIL-88(Fe) and NH_2-MIL-88(Fe) respectively, at the 5th cycles. The kinetics and isotherms studies were more favored by the pseudo-second-order and Langmuir models respectively, suggesting the good adsorption capacity of the MOFs. Thermodynamic data reveal the exothermic nature of the overall process. Molecular docking simulations predicted better interactions between CRY and MIL-88(Fe) MOF which was well agreed with the experimental findings. In comparison to previous reports in the literature, the MOFs were proven to be clearly superior especially in terms of rapid equilibration (25 minutes), % R (95.2 - 98.9%) and ease of regeneration. In summary, MIL-88(Fe) and NH_2-MIL-88(Fe) MOFs are promising adsorbents that deserve serious consideration for the effective removal of environmental pollutants such as CRY.

Acknowledgments

This research work is fully sponsored by YUTP grant provided by Universiti Teknologi PETRONAS with cost center number 015LCO-071 and the UTP-UIR International Grant with cost center 015MEO-038.

References

[1] Z. Kong, L. Li, Y. Xue, M. Yang, Y.-Y. Li, Challenges and prospects for the anaerobic treatment of chemical-industrial organic wastewater: A review, J. Clean. Prod. 231 (2019) 913–927. doi:10.1016/j.jclepro.2019.05.233.

[2] H. Shang, Z. Sun, PAHs (naphthalene) removal from stormwater runoff by organoclay amended pervious concrete, Constr. Build. Mater. 200 (2019) 170–180. doi:10.1016/j.conbuildmat.2018.12.096.

[3] A. Zeneli, E. Kastanaki, F. Simantiraki, E. Gidarakos, Monitoring the biodegradation of TPH and PAHs in refinery solid waste by biostimulation and bioaugmentation, J. Environ. Chem. Eng. 7 (2019). doi:10.1016/j.jece.2019.103054.

[4] I. Bouzid, J. Maire, E. Brunol, S. Caradec, N. Fatin-Rouge, Compatibility of surfactants with activated-persulfate for the selective oxidation of PAH in groundwater remediation, J. Environ. Chem. Eng. 5 (2017) 6098–6106. doi:10.1016/j.jece.2017.11.038.

[5] L. Zhao, J. Deng, H. Hou, J. Li, Y. Yang, Investigation of PAH and oil degradation along

with electricity generation in soil using an enhanced plant-microbial fuel cell, J. Clean. Prod. 221 (2019) 678–683. doi:10.1016/j.jclepro.2019.02.212.

[6] A. Balati, M. Ghanbari, S.K. Behzad, M.M. Amini, Functionalization of graphene oxide with 9-aminoanthracene for the adsorptive removal of persistent aromatic pollutants from aqueous solution, Acta Chim. Slov. (2017) 479–490. doi:10.17344/acsi.2017.3372.

[7] H. Li, R. Qu, C. Li, W. Guo, X. Han, F. He, Y. Ma, B. Xing, Selective removal of polycyclic aromatic hydrocarbons (PAHs) from soil washing effluents using biochars produced at different pyrolytic temperatures, Bioresour. Technol. 163 (2014) 193–198. doi:10.1016/j.biortech.2014.04.042.

[8] M. Rani, U. Shanker, Enhanced photocatalytic degradation of chrysene by Fe_2O_3 @ ZnHCF nanocubes, Chem. Eng. J. 348 (2018) 754–764. doi:10.1016/j.cej.2018.04.185.

[9] L.H. Tran, P. Drogui, G. Mercier, J.F. Blais, Coupling extraction-flotation with surfactant and electrochemical degradation for the treatment of PAH contaminated hazardous wastes, J. Hazard. Mater. 170 (2009) 1218–1226. doi:10.1016/j.jhazmat.2009.05.104.

[10] A.D.L. Wickramasinghe, S.P. Shukla, Performance evaluation of a pellet based column bed for removal of a potentially carcinogenic polycyclic aromatic hydrocarbon (PAH) from water, J. Environ. Chem. Eng. 6 (2018) 6012–6020. doi:10.1016/j.jece.2018.09.009.

[11] Y. Dai, J. Niu, L. Yin, J. Xu, Y. Xi, Sorption of polycyclic aromatic hydrocarbons on electrospun nanofibrous membranes: Sorption kinetics and mechanism, J. Hazard. Mater. 192 (2011) 1409–1417. doi:10.1016/j.jhazmat.2011.06.055.

[12] E. chun Pan, H. Sun, Q. jin Xu, Q. Zhang, L. fei Liu, X. dong Chen, Y. Xu, Polycyclic

aromatic hydrocarbons concentrations in drinking water in Villages along the Huai River in China and their association with high cancer incidence in local population, Biomed Res. Int. 2015 (2015) 1–10. doi:10.1155/2015/762832.

[13] S.R. Barman, P. Banerjee, A. Mukhopadhayay, P. Das, Biodegradation of acenapthene and naphthalene by *Pseudomonas mendocina*: Process optimization, and toxicity evaluation, J. Environ. Chem. Eng. 5 (2017) 4803–4812. doi:10.1016/j.jece.2017.09.012.

[14] M.J. Alessandrello, E.A. Parellada, M.S. Juárez Tomás, A. Neske, D.L. Vullo, M.A. Ferrero, Polycyclic aromatic hydrocarbons removal by immobilized bacterial cells using annonaceous acetogenins for biofilm formation stimulation on polyurethane foam, J. Environ. Chem. Eng. 5 (2017) 189–195. doi:10.1016/j.jece.2016.11.037.

[15] M.M. Kgatitsoe, S. Ncube, H. Tutu, I.A. Nyambe, L. Chimuka, Synthesis and characterization of a magnetic nanosorbent modified with *Moringa oleifera* leaf extracts for removal of nitroaromatic explosive compounds in water samples, J. Environ. Chem. Eng. 7 (2019). doi:10.1016/j.jece.2019.103128.

[16] A. Akcil, C. Erust, S. Ozdemiroglu, V. Fonti, F. Beolchini, A review of approaches and techniques used in aquatic contaminated sediments: Metal removal and stabilization by chemical and biotechnological processes, J. Clean. Prod. 86 (2015) 24–36. doi:10.1016/j.jclepro.2014.08.009.

[17] J. Wang, S. Wang, Preparation, modification and environmental application of biochar: A review, J. Clean. Prod. 227 (2019) 1002–1022. doi:10.1016/j.jclepro.2019.04.282.

[18] X. Ge, Z. Wu, Z. Wu, Y. Yan, G. Cravotto, B. Ye, Enhanced PAHs adsorption using iron-modified coal-based activated carbon via microwave radiation, J. Taiwan Chem. Eng, 64

(2016) 235–243. doi:10.1016/j.jtice.2016.03.050.

[19] G. Patra, R. Barnwal, S.K. Behera, B.C. Meikap, Removal of dyes from aqueous solution by sorption with fly ash using a hydrocyclone, J. Environ. Chem. Eng. 6 (2018) 5204–5211. doi:10.1016/j.jece.2018.08.011.

[20] M. Changmai, P. Banerjee, K. Nahar, M.K. Purkait, A novel adsorbent from carrot, tomato and polyethylene terephthalate waste as a potential adsorbent for Co (II) from aqueous solution: Kinetic and equilibrium studies, J. Environ. Chem. Eng. 6 (2018) 246–257. doi:10.1016/j.jece.2017.12.009.

[21] Z. Uba Zango, S. Shehu Imam, Evaluation of microcrystalline cellulose from groundnut shell for the removal of crystal violet and methylene Blue, Nanosci. Nanotechnol. 8 (2018) 1–6. doi:10.5923/j.nn.20180801.01.

[22] U.L. Muhammad, Z.U. Zango, H.A. Kadir, Crystal violet removal from aqeous solution using corn stalk biosorbent, Sci. World J. 14 (2019) 133–138.

[23] A. Macías-García, J.P. Carrasco-Amador, V. Encinas-Sánchez, M.A. Díaz-Díez, D. Torrejón-Martín, Preparation of activated carbon from kenaf by activation with H_3PO_4. Kinetic study of the adsorption/electroadsorption using a system of supports designed in 3D, for environmental applications, J. Environ. Chem. Eng. 7 (2019). doi:10.1016/j.jece.2019.103196.

[24] Z.N. Garba, Z.U. Zango, A.A. Babando, A. Galadima, Competitive adsorption of dyes onto granular activated carbon, J. Chem. Pharm. Res. 7 (2015) 710–717. www.jocpr.com.

[25] M.H. Al-Malack, M. Dauda, Competitive adsorption of cadmium and phenol on activated

carbon produced from municipal sludge, J. Environ. Chem. Eng. 5 (2017) 2718–2729. doi:10.1016/j.jece.2017.05.027.

[26] P.A. Alaba, N.A. Oladoja, Y.M. Sani, O. Bolarinwa, I. Yakub, S. Felix, Insight into wastewater decontamination using polymeric adsorbents, J. Environ. Chem. Eng. 6 (2018) 1651–1672. doi:10.1016/j.jece.2018.02.019.

[27] L. Guo, Y. Zeng, A. Guan, G. Chen, Reactive & functional polymers preparation and characterization of molecularly imprinted silica particles for selective adsorption of naphthalene, React. Funct. Polym. 71 (2011) 1172–1176. doi:10.1016/j.reactfunctpolym.2011.08.005.

[28] A.Y.W. Sham, S.M. Notley, Adsorption of organic dyes from aqueous solutions using surfactant exfoliated graphene, J. Environ. Chem. Eng. 6 (2018) 495–504. doi:10.1016/j.jece.2017.12.028.

[29] X. Wang, P. Tang, C. Ding, X. Cao, S. Yuan, X. Zuo, X. Deng, Simultaneous enhancement of adsorption and peroxymonosulfate activation of nitrogen-doped reduced graphene oxide for bisphenol A removal, J. Environ. Chem. Eng. 5 (2017) 4291–4297. doi:10.1016/j.jece.2017.08.018.

[30] Y. Liu, H. Huang, D. Gan, L. Guo, M. Liu, J. Chen, F. Deng, N. Zhou, X. Zhang, Y. Wei, A facile strategy for preparation of magnetic graphene oxide composites and their potential for environmental adsorption, Ceram. Int. 44 (2018) 18571–18577. doi:10.1016/j.ceramint.2018.07.081.

[31] X. Wang, B. Liu, Q. Lu, Q. Qu, Graphene-based materials : Fabrication and application for adsorption in analytical chemistry, J. Chromatogr. A. 1362 (2014) 1–15.

doi:10.1016/j.chroma.2014.08.023.

[32] Z.U. Zango, N.H.H. Abu Bakar, W.L. Tan, M.A. Bakar, Enhanced removal efficiency of methyl red via the modification of halloysite nanotubes by copper oxide, J. Dispers. Sci. Technol. (2017). doi:10.1080/01932691.2017.1301259.

[33] Z.U. Zango, Z.N. Garba, N.H.H. Abu Bakar, W.L. Tan, M. Abu Bakar, Adsorption studies of Cu^{2+}–Hal nanocomposites for the removal of 2,4,6-trichlorophenol, Appl. Clay Sci. 132–133 (2016) 68–78. doi:10.1016/j.clay.2016.05.016.

[34] A. Mohammadi, P. Veisi, High adsorption performance of β-cyclodextrin-functionalized multi-walled carbon nanotubes for the removal of organic dyes from water and industrial wastewater, J. Environ. Chem. Eng. 6 (2018) 4634–4643. doi:10.1016/j.jece.2018.07.002.

[35] J. Dou, D. Gan, Q. Huang, M. Liu, J. Chen, F. Deng, X. Zhu, Y. Wen, X. Zhang, Y. Wei, Functionalization of carbon nanotubes with chitosan based on MALI multicomponent reaction for Cu^{2+} removal, Int. J. Biol. Macromol. 136 (2019) 476–485. doi:10.1016/j.ijbiomac.2019.06.112.

[36] X. Zhang, Q. Huang, M. Liu, J. Tian, G. Zeng, Z. Li, K. Wang, Q. Zhang, Q. Wan, F. Deng, Y. Wei, Preparation of amine functionalized carbon nanotubes via a bioinspired strategy and their application in Cu^{2+} removal, Appl. Surf. Sci. 343 (2015) 19–27. doi:10.1016/j.apsusc.2015.03.081.

[37] J. Huang, H. Liu, S. Chen, C. Ding, Hierarchical porous MWCNTs-silica aerogel synthesis for high-efficiency oily water treatment, J. Environ. Chem. Eng. 4 (2016) 3274–3282. doi:10.1016/j.jece.2016.06.039.

[38] J.O. Otalvaro, M. Avena, M. Brigante, Adsorption of organic pollutants by amine functionalized mesoporous silica in aqueous solution. effects of pH, ionic strength and some consequences of APTES stability, J. Environ. Chem. Eng. 7 (2019) 103325. doi:10.1016/j.jece.2019.103325.

[39] J. Benvenuti, A. Fisch, J.H.Z. dos Santos, M. Gutterres, Silica-based adsorbent material with grape bagasse encapsulated by the sol-gel method for the adsorption of Basic Blue 41 dye, J. Environ. Chem. Eng. 7 (2019) 103342. doi:10.1016/j.jece.2019.103342.

[40] Q. Huang, M. Liu, J. Chen, Q. Wan, J. Tian, L. Huang, R. Jiang, Y. Wen, X. Zhang, Y. Wei, Facile preparation of MoS_2 based polymer composites via mussel inspired chemistry and their high efficiency for removal of organic dyes, Appl. Surf. Sci. 419 (2017) 35–44. doi:10.1016/j.apsusc.2017.05.006.

[41] Q. Huang, M. Liu, L. Mao, D. Xu, G. Zeng, H. Huang, R. Jiang, F. Deng, X. Zhang, Y. Wei, Surface functionalized SiO_2 nanoparticles with cationic polymers via the combination of mussel inspired chemistry and surface initiated atom transfer radical polymerization: Characterization and enhanced removal of organic dye, J. Colloid Interface Sci. 499 (2017) 170–179. doi:10.1016/j.jcis.2017.03.102.

[42] X. Zhang, Q. Huang, F. Deng, H. Huang, Q. Wan, M. Liu, Y. Wei, Mussel-inspired fabrication of functional materials and their environmental applications: Progress and prospects, Appl. Mater. Today. 7 (2017) 222–238. doi:10.1016/j.apmt.2017.04.001.

[43] Z. Luo, S. Fan, J.L. Id, W. Liu, X. Shen, C. Wu, polymers A 3D Stable Metal–Organic framework for highly Eeficient adsorption and removal of drug contaminants from water, (2018) 12–18. doi:10.3390/polym10020209.

[44] J. Li, Z. Wu, Q. Duan, A. Alsaedi, T. Hayat, C. Chen, Decoration of ZIF-8 on polypyrrole nanotubes for highly efficient and selective capture of U(VI), J. Clean. Prod. 204 (2018) 896–905. doi:10.1016/j.jclepro.2018.09.050.

[45] M. Oveisi, N.M. Mahmoodi, M.A. Asli, Facile and green synthesis of metal-organic framework/inorganic nanofiber using electrospinning for recyclable visible-light photocatalysis, J. Clean. Prod. 222 (2019) 669–684. doi:10.1016/j.jclepro.2019.03.066.

[46] L. Fu, S. Wang, G. Lin, L. Zhang, Q. Liu, H. Zhou, C. Kang, S. Wan, H. Li, S. Wen, Post-modification of UiO-66-NH2 by resorcyl aldehyde for selective removal of Pb(II) in aqueous media, J. Clean. Prod. 229 (2019) 470–479. doi:10.1016/j.jclepro.2019.05.043.

[47] S. Dhaka, R. Kumar, A. Deep, M.B. Kurade, S.W. Ji, B.H. Jeon, Metal–organic frameworks (MOFs) for the removal of emerging contaminants from aquatic environments, Coord. Chem. Rev. 380 (2019) 330–352. doi:10.1016/j.ccr.2018.10.003.

[48] T. Van Tran, V.D. Cao, V.H. Nguyen, B.N. Hoang, D.V.N. Vo, T.D. Nguyen, L.G. Bach, MIL-53 (Fe) derived magnetic porous carbon as a robust adsorbent for the removal of phenolic compounds under the optimized conditions, J. Environ. Chem. Eng. 53 (2019). doi:10.1016/j.jece.2019.102902.

[49] B. Xu, H. Yang, Y. Cai, H. Yang, C. Li, Preparation and photocatalytic property of spindle-like MIL-88B(Fe) nanoparticles, Inorg. Chem. Commun. 67 (2016) 29–31. http://dx.doi.org/10.1016/j.inoche.2016.03.003.

[50] A. Bonilla-Petriciolet, D.I.M.-C. HildaElizabethReynel-Ávila, Adsorption processes for water treatment, 2017. doi:10.2337/dc12-1077.

[51] G.L. Dotto, J.A.V. Costa, L.A.A. Pinto, Kinetic studies on the biosorption of phenol by nanoparticles from Spirulina sp. LEB 18, J. Environ. Chem. Eng. 1 (2013) 1137–1143. doi:10.1016/j.jece.2013.08.029.

[52] L.N. Nthunya, L. Gutierrez, S. Derese, B.B. Mamba, A.R. Verliefde, S.D. Mhlanga, Adsorption of phenolic compounds by polyacrylonitrile nanofibre membranes: A pretreatment for the removal of hydrophobic bearing compounds from water, J. Environ. Chem. Eng. 7 (2019) 103254. doi:10.1016/j.jece.2019.103254.

[53] H.S. Jamwal, S. Kumari, G.S. Chauhan, N.S. Reddy, J.H. Ahn, Silica-polymer hybrid materials as methylene blue adsorbents, J. Environ. Chem. Eng. 5 (2017) 103–113. doi:10.1016/j.jece.2016.11.029.

[54] A.T. Babu, R. Antony, Green synthesis of silver doped nano metal oxides of zinc & copper for antibacterial properties, adsorption, catalytic hydrogenation & photodegradation of aromatics, J. Environ. Chem. Eng. 7 (2019). doi:10.1016/j.jece.2018.102840.

[55] T.C. Perrotti, N.S. Freitas, M. Alzamora, D.R. Sánchez, N.M.F. Carvalho, Green iron nanoparticles supported on amino-functionalized silica for removal of the dye methyl orange, J. Environ. Chem. Eng. 7 (2019) 103237. doi:10.1016/j.jece.2019.103237.

[56] E.C. Peres, J.C. Slaviero, A.M. Cunha, A. Hosseini-Bandegharaei, G.L. Dotto, Microwave synthesis of silica nanoparticles and its application for methylene blue adsorption, J. Environ. Chem. Eng. 6 (2018) 649–659. doi:10.1016/j.jece.2017.12.062.

[57] A.K. Malde, L. Zuo, M. Breeze, M. Stroet, D. Poger, P.C. Nair, C. Oostenbrink, A.E. Mark, An automated force field topology builder (ATB) and repository: Version 1.0, J. Chem. Theory Comput. 7 (2011) 4026–4037. doi:10.1021/ct200196m.

[58] J. Fuhrmann, A. Rurainski, H.-P. Lenhof, D. Neumann, A new Lamarckian genetic algorithm for flexible ligand-receptor docking, J. Comput. Chem. 31 (2010) 1911–1918. doi:10.1002/jcc.21478.

[59] E. Rahmani, M. Rahmani, Alkylation of benzene over Fe-based metal organic frameworks (MOFs) at low temperature condition, Microporous Mesoporous Mater. 249 (2017) 118–127. doi:10.1016/j.micromeso.2017.04.058.

[60] S.Y. Guo, Hongxu Baitong Niu, Xuemin Wu, Yi Zhang, Effective removal of 2,4,6-trinitrophenol over hexagonal metal–organic framework NH_2- MIL- 88B(Fe), Appl. Organomet. Chem. (2018) 1–11. doi:10.1002/aoc.4580.

[61] X. Li, J. Zhang, W. Shen, S. Xu, Rapid synthesis of metal-organic frameworks MIL-53(Cr), 255 (2019) 2–4.

[62] L. Wang, L. Zan, WO_3 into MIL-101 for enhancement charge carrier separation of photocatalyst, Sci. Rep. 9 (2019) 1–11. doi:10.1038/s41598-019-41374-z.

[63] J. He, Y. Zhang, X. Zhang, Y. Huang, Highly efficient Fenton and enzyme-mimetic activities of NH_2-MIL-88B(Fe metal organic framework for methylene blue degradation, Sci. Rep. (2018) 1–8. doi:10.1038/s41598-018-23557-2.

[64] D.T. Sponza, R. Oztekin, Removals of some hydrophobic poly aromatic hydrocarbons (PAHs) and *Daphnia magna* acute toxicity in a petrochemical industry wastewater with ultrasound in Izmir-Turkey, Sep. Purif. Technol. 77 (2011) 301–311. doi:10.1016/j.seppur.2010.12.021.

[65] F.S. and U.R.D. Maryam Abbasi, Preparation of Silver Nanoparticles from Synthetic and

Natural Sources : Remediation Model for PAHs Preparation of Silver Nanoparticles from Synthetic and Natural Sources : Remediation model for PAHs, Int. Symp. Adv. Mater. (ISAM 2013). (2013). doi:10.1088/1757-899X/60/1/012061.

[66] Z. Hao, C. Wang, Z. Yan, H. Jiang, H. Xu, Magnetic particles modification of coconut shell-derived activated carbon and biochar for effective removal of phenol from water, Chemosphere. 211 (2018) 962–969. doi:10.1016/j.chemosphere.2018.08.038.

[67] J. Lladó, R.R. Gil, C. Lao-Luque, M. Solé-Sardans, E. Fuente, B. Ruiz, Highly microporous activated carbons derived from biocollagenic wastes of the leather industry as adsorbents of aromatic organic pollutants in water, J. Environ. Chem. Eng. 5 (2017) 2090–2100. doi:10.1016/j.jece.2017.04.018.

[68] V.W.O. Wanjeri, C.J. Sheppard, A.R.E. Prinsloo, J.C. Ngila, P.G. Ndungu, Isotherm and kinetic investigations on the adsorption of organophosphorus pesticides on graphene oxide based silica coated magnetic nanoparticles functionalized with 2-phenylethylamine, J. Environ. Chem. Eng. 6 (2018) 1333–1346. doi:10.1016/j.jece.2018.01.064.

[69] N.A.S. Mohammed, R.A. Abu-Zurayk, I. Hamadneh, A.H. Al-Dujaili, Phenol adsorption on biochar prepared from the pine fruit shells: Equilibrium, kinetic and thermodynamics studies, J. Environ. Manage. 226 (2018) 377–385. doi:10.1016/j.jenvman.2018.08.033.

[70] A. Rosińska, L. Dabrowska, Selection of coagulants for the removal of chosen PAH from drinking water, Water (Switzerland). 10 (2018). doi:10.3390/w10070886.

[71] R.J. Krupadam, Nanoporous polymeric material for remediation of PAHs polluted water, Polycycl. aromat. compd. 32 (2012) 313–333. doi:10.1080/10406638.2011.633591.

[72] U.A. Patrick, E.C. Christain, Adsorption and distribution of selected high molecular weight polycyclic aromatic hydrocarbons in a typical coastal sand deposit, Am. J. Eng. Appl. Sci. 11 (2018) 368–378. doi:10.3844/ajeassp.2018.368.378.

[73] M. Ma, H. Noei, B. Mienert, J. Niesel, E. Bill, M. Muhler, R.A. Fischer, Y. Wang, U. Schatzschneider, N. Metzler-Nolte, Iron metal-organic frameworks MIL-88B and NH2-MIL-88B for the loading and delivery of the gasotransmitter carbon monoxide, Chem. - A Eur. J. 19 (2013) 6785–6790. doi:10.1002/chem.201201743.

Table 1: Surface area, pore volume and pore size of MIL-88(Fe) and NH_2-MIL-88(Fe) MOFs

Properties	**MIL-88(Fe)**	**NH_2-MIL-88(Fe)**
BET surface area ($m^2\ g^{-1}$)	1242	941
Micropores surface area ($m^2\ g^{-1}$)	761	749
Pore volume ($m^3\ g^{-1}$)	0.7	0.6
Particle sizes (nm)	12.5	8.8

Table 2: Kinetics parameters for the adsorption of CRY onto the MOFs

Kinetic Models		MIL-88(Fe)	NH_2-MIL-88(Fe)
	$q_{e,exp}$ (mg g^{-1})	23.60	22.2
Pseudo-first-order model	$q_{e,cal}$ (mg g^{-1})	7.129	1.538
	K_1 (min^{-1})	1.109	1.167
	R^2	0.573	0.502
	R^2 adj	0.512	0.431
	RMSE	5.086	4.818
	AIC	31.017	30.040
Pseudo-second-order model	$q_{e,cal}$ (mg g^{-1})	21.876	20.450
	K_2 (g mg^{-1} min^{-1})	0.006	0.005
	R^2	0.996	0.998
	R^2 adj	0.998	0.998
	RMSE	0.037	0.028
	AIC	-57.443	-62.315
Intra-particle diffusion model	K_p (mg^{-1} g^{-1} $min^{1/2}$)	0.80	0.66
	C	10.31	9.91
	R^2	0.573	0.502
	R^2 adj	0.512	0.431
	RMSE	5.086	4.818
	AIC	31.017	30.040

Table 3: Thermodynamic parameters for the adsorption of CRY onto the MOFs

	MIL-88(Fe)					**NH_2-MIL-88(Fe)**				
Temp (K)	ΔG° ((KJ mol^{-1})	ΔH° (K J mol^{-1})	ΔS° (J mol^{-1} K^{1})	SD	RSD	ΔG° (KJ mol^{-1})	ΔH° (J mol^{-1} K)	ΔS° (K J mol^{-1})	SD	RSD
298	– 11.30			±0.001	±1.634	– 8.92			±0.002	±4.225
308	– 10.17	– 28.31	– 57.86	±0.001	±1.493	– 8.92	– 15.18	– 20.69	±0.001	±2.665
318	– 9.91			±0.002	±3.849	– 8.70			±0.002	±4.499
328	– 9.38			±0.001	±1.076	– 8.34			±0.001	±1.769
338	– 8.82			±0.002	±2.887	– 8.17			±0.001	±1.000

Table 4: Comparisons of various adsorbents materials used for the removals of CRY

Adsorbent materials	**Equilibrium time**	**Q_{max} (mg g^{-1})**	**Percentage removal**	**Reference**
Powdered activated carbon	15 minutes	Not mentioned	66.5	[70]
Nanoporous polymeric material	3 hours	4.89	90.0	[71]
Commercial activated carbon	3 hours	0.78	60.0	[71]
Coastal sand	28 days	1.95×10^{-3}	56.7	[72]
MIL-88(Fe) MOF	25 minutes	23.6±0.001	98.9	This work
NH_2-MIL-88(Fe) MOF	25 minutes	22.2±0.001	95.2	This work